

DRAFT VERSION NOVEMBER 17, 2021
Typeset using L^AT_EX preprint2 style in AASTeX63

AGILE Observations of Fast Radio Bursts

F. VERRECCHIA,^{1,2} C. CASENTINI,^{3,4} M. TAVANI,^{3,5} A. URSI,³ S. MEREGHETTI,⁶ M. PILIA,⁷
M. CARDILLO,³ A. ADDIS,⁸ G. BARBIELLINI,⁹ L. BARONCELLI,^{8,10} A. BULGARELLI,⁸
P.W. CATTANEO,¹¹ A. CHEN,¹² E. COSTA,³ E. DEL MONTE,³ A. DI PIANO,⁸ A. FERRARI,¹³
V. FIORETTI,⁸ F. LONGO,⁹ F. LUCARELLI,^{1,2} N. PARMIGGIANI,^{8,14} G. PIANO,³ C. PITTORI,^{1,2}
A. RAPPOLDI,¹¹ AND S. VERCELLONE¹⁵

¹SSDC/ASI, via del Politecnico snc, I-00133 Roma (RM), Italy

²INAF/OAR, via Frascati 33, I-00078 Monte Porzio Catone (RM), Italy

³INAF/IAPS, via del Fosso del Cavaliere 100, I-00133 Roma (RM), Italy

⁴INFN Sezione di Roma 2, via della Ricerca Scientifica 1, I-00133 Roma (RM), Italy

⁵Università degli Studi di Roma Tor Vergata, via della Ricerca Scientifica 1, I-00133 Roma (RM), Italy

⁶INAF/IASF, via E. Bassini 15, I-20133 Milano (MI), Italy

⁷INAF/OAC, via della Scienza 5, I-09047 Selargius (CA), Italy

⁸INAF/OAS, via Gobetti 101, I-40129 Bologna (BO), Italy

⁹Dipartimento di Fisica, Università di Trieste and INFN, via Valerio 2, I-34127 Trieste (TS), Italy

¹⁰Dip. di Fisica e Astronomia, Università di Bologna, Viale Berti Pichat 6/2, 40127, Bologna, Italy

¹¹INFN Sezione di Pavia, via U. Bassi 6, I-27100 Pavia (PV), Italy

¹²School of Physics, Wits University, Johannesburg, South Africa

¹³CIFS, c/o Physics Department, University of Turin, via P. Giuria 1, I-10125, Torino, Italy

¹⁴Università degli Studi di Modena e Reggio Emilia, DIFE - Via Pietro Vivarelli 10, 41125 Modena, Italy

¹⁵INAF/OAB, via E. Bianchi 46, I-23807 Merate (LC), Italy

(Received December 22, 2020; Revised April 29, 2021; Accepted April 29, 2021)

Submitted to ApJ

ABSTRACT

We report on a systematic search for hard X-ray and γ -ray emission in coincidence with fast radio bursts (FRBs) observed by the AGILE satellite. We used 13 yr of AGILE archival data searching for time coincidences between exposed FRBs and events detectable by the MCAL (0.4-100 MeV) and GRID (50 MeV-30 GeV) detectors at timescales ranging from milliseconds to days/weeks. The current AGILE sky coverage allowed us to extend the search for high-energy emission preceding and following the FRB occurrence. We considered all FRBs sources currently included in catalogs, and identified a subsample (15 events) for which a good AGILE exposure either with MCAL or GRID was obtained. In this paper we focus on nonrepeating FRBs, compared to a few nearby repeating sources. We did not detect significant MeV or GeV emission from any event. Our hard X-ray upper limits (ULs) in the MeV energy

francesco.verrecchia@inaf.it

claudio.casentini@inaf.it

marco.tavani@inaf.it

range were obtained for timescales from submillisecond to seconds, and in the GeV range from minutes to weeks around event times. We focus on a subset of five non-repeating and two repeating FRB sources whose distances are most likely smaller than that of 180916.J0158+65 (150 Mpc). For these sources, our MeV ULs translate into ULs on the isotropically emitted energy of about 3×10^{46} erg, comparable to that observed in the 2004 giant flare from the Galactic magnetar SGR 1806-20. On average, these nearby FRBs emit radio pulses of energies significantly larger than the recently detected SGR 1935+2154 and are not yet associated with intense MeV flaring.

Keywords: fast radio burst, gamma rays: general.

1. INTRODUCTION

Fast radio bursts (FRBs) are transient events of unknown origin consisting of bright millisecond radio pulses at ~ 1 GHz having usually large dispersion measures (DMs; the free electron density along the line of sight at a certain distance) in excess of Galactic values (Lorimer et al. 2007; Katz 2019; Petroff et al. 2019, and Cordes & Chatterjee 2019, hereafter CC19). The sources known so far, 110 as of 2020 May 1 (see FRBCAT¹ Petroff et al. 2016, and the CHIME/FRB telescope public on-line database²), have an isotropic sky distribution and for most of them a single radio burst was detected. A smaller, but increasing number of FRBs show repeating pulses (Spitler et al. 2016), which usually occur erratically in time, and two of them show a periodic pattern in their activity cycle, as in the case of FRB 180916.J0158+65 (CHIME/FRB Collaboration et al. 2020, hereafter C20). No clear evidence for physically different populations distinguishing repeating and nonrepeating sources has been obtained so far. The FRB distances can be deduced from their DM measures, which are typically $DM \geq 500 \text{ pc cm}^{-3}$, which, taking into account Galactic and extragalactic contributions, point to an extragalactic origin. The short duration of FRBs (typically milliseconds or less)

favors models involving compact objects such as strongly magnetized neutron stars (magnetars) and massive black holes (Platts et al. 2019).

Since 2019 the CHIME/FRB collaboration has reported the discovery of several repeating FRBs (hereafter R-FRBs; CHIME/FRB Collaboration et al. 2019a,b,c, hereafter C19; Fonseca et al. 2020), with DM ranging from 103.5 to 1378 pc cm^{-3} . The characteristics of this sample of R-FRBs are particularly interesting for counterpart searches, as we discussed in Casentini et al. 2020, focused on two nearby sources, 180916.J0158+65 (Source 1, following the nomenclature of C19) and 181030.J1054+73 (Source 2). These two sources have low DM values in excess of their respective Galactic disk and halo contributions (see next section) and are therefore expected to be relatively close to Earth (as confirmed by the redshift-determined distance of Source 1 equal to 149 Mpc; Marcote et al. 2020, hereafter M20). As we will see, this distance determination for a prominent FRB sets the scale for our discussion on the implications of our search for high-energy emission from FRBs. Source 1 has been recently reported to have periodic bursting activity (C20), with most radio bursts emitted within time intervals recurring periodically every 16.3 days (Pleunis et al. 2021). A multifrequency follow-up campaign has been organized to search for high-energy and optical emission during active

¹ <http://www.frbcat.org/>

² <https://www.chime-frb.ca>

Table 1. FRB Catalog Sources.

ID	DATE UTC	L/H (deg)	B/H (deg)	DM and Error (cm^{-3} pc)	Radio Fluence (Jy ms)	Within MCAL FOV	Within GRID FOV	Within Super-A FOV	Off-axis Angle (deg)	Repeater
090625	2009-06-25 21:53:51.379	226.44	-60.03	899.55 ± 0.01	2.189	YES	NO	NO	94.91	NO
110214	2011-02-14 07:14:10.353	290.70	-66.60	168.9 ± 0.5	51.300	YES	YES	NO	63.02	NO
110220	2011-02-20 01:55:48.096	50.83	-54.77	944.38 ± 0.05	7.310	NO	NO	NO	93.94	NO
110523	2011-05-23 15:06:19.700	56.12	-37.82	623.3 ± 0.06	1.038	YES	YES	NO	44.12	NO
110626	2011-06-26 21:33:17.477	355.86	-41.75	723.0 ± 0.3	0.560	NO	NO	NO	128.61	NO
110703	2011-07-03 18:59:40.607	81.00	-59.02	1103.6 ± 0.7	1.750	NO	NO	NO	157.70	NO
120127	2012-01-27 08:11:21.725	49.29	-66.20	553.3 ± 0.3	0.750	-	-	-	-	NO
121002	2012-10-02 13:09:18.436	308.22	-26.26	1629.18 ± 0.02	2.280	YES	YES	NO	63.80	NO
121102	2012-11-02 06:35:53.244	174.95	-0.23	557 ± 2	1.200	NO	NO	NO	133.28	YES
130626	2013-06-26 14:55:59.771	7.45	27.42	952.4 ± 0.1	> 1.500	-	-	-	-	NO
130628	2013-06-28 03:58:00.178	225.96	30.66	469.88 ± 0.01	> 1.220	YES	YES	NO	50.26	NO
130729	2013-07-29 09:01:51.190	324.79	54.74	861 ± 2	> 3.5	NO	NO	NO	67.85	NO
131104	2013-11-04 18:04:11.200	260.55	-21.93	779 ± 1	2.750	-	-	-	-	NO
140514	2014-05-14 17:14:11.060	50.84	-54.61	562.7 ± 0.6	1.320	NO	NO	NO	144.34	NO
141113	2014-11-13 07:42:55.220	191.90	0.36	400.3	0.078	YES	YES	NO	61.39	NO
150215	2015-02-15 20:41:41.714	24.66	5.28	1105.6 ± 0.8	2.020	-	-	-	-	NO
150418	2015-04-18 04:29:06.657	232.67	-3.23	776.2 ± 0.5	1.760	NO	NO	NO	161.08	NO
150610	2015-06-10 05:26:59.396	278.00	16.50	1593.9 ± 0.6	1.300	YES	NO	NO	141.61	NO
150807	2015-08-07 17:53:55.830	333.89	-53.60	266.5 ± 0.1	44.800	NO	NO	NO	49.49	NO
151206	2015-12-06 06:17:52.778	32.60	-8.50	1909.8 ± 0.6	0.900	NO	NO	NO	63.28	NO
151230	2015-12-30 16:15:46.525	239.00	34.80	960.4 ± 0.5	1.900	YES	NO	NO	90.33	NO
160102	2016-01-02 08:28:39.374	18.90	-60.80	2596.1 ± 0.3	1.800	NO	NO	NO	44.87	NO
160317	2016-03-17 09:00:36.530	246.05	-0.99	1165 ± 11	63.000	NO	NO	NO	61.41	NO
160410	2016-04-10 08:33:39.680	220.36	27.19	278 ± 3	28.000	NO	NO	NO	32.96	NO
160608	2016-06-08 03:53:01.088	254.11	-9.54	682 ± 7	38.700	NO	NO	NO	165.22	NO
170107	2017-01-07 20:05:08.139	266.08	51.45	609.5 ± 0.5	58.000	YES	YES	YES	29.45	NO
170416	2017-04-16 23:11:12.799	337.62	-50.05	523.2 ± 0.2	97.000	YES	NO	NO	133.52	NO
170428	2017-04-28 18:02:34.700	326.75	-41.85	991.7 ± 0.9	34.000	YES	NO	NO	122.82	NO
170707	2017-07-07 06:17:34.354	275.02	-52.39	235.2 ± 0.6	52.000	YES	YES	NO	50.66	NO
170712	2017-07-12 13:22:17.394	327.41	-49.24	312.79 ± 0.07	53.000	YES	NO	NO	104.46	NO

Table 1 continued

Table 1 (*continued*)

ID	DATE UTC	LII (deg)	BII (deg)	DM and Error (cm^{-3}pc)	Radio Fluence (Jy ms)	Within MCAL FOV	Within GRID FOV	Within Super-A FOV	Off-axis Angle (deg)	Repeater
170827	2017-08-27 16:20:18.000	303.20	-51.70	176.80 ± 0.04	19.870	NO	NO	NO	81.31	NO
170906	2017-09-06 13:06:56.488	33.85	-50.20	390.3 ± 0.4	74.000	YES	NO	NO	73.37	NO
170922	2017-09-22 11:23:33.400	45.10	-38.70	1111 ± 1	177.000	YES	NO	NO	128.74	NO
171003	2017-10-03 04:07:23.781	294.90	48.41	463.2 ± 1.2	81.000	YES	NO	NO	95.98	NO
171004	2017-10-04 03:23:39.250	282.69	48.84	304.0 ± 0.3	44.000	YES	NO	NO	79.72	NO
171019	2017-10-19 13:26:40.097	52.51	-49.24	460.8 ± 1.1	219.000	YES	NO	NO	134.78	NO
171020	2017-10-20 10:27:58.598	36.17	-53.49	114.1 ± 0.2	200.000	NO	NO	NO	80.64	NO
171116	2017-11-16 14:59:33.305	206.37	-51.93	618.5 ± 0.5	63.000	YES	NO	NO	95.06	NO
171209	2017-12-09 20:34:23.500	332.20	6.24	1457.40 ± 0.03	3.700	YES	NO	NO	105.10	NO
171213	2017-12-13 14:22:40.467	198.85	-47.48	158.6 ± 0.2	133.000	YES	NO	NO	126.69	NO
171216	2017-12-16 17:59:10.822	271.19	-49.29	203.1 ± 0.5	40.000	NO	NO	NO	30.35	NO
180110	2018-01-10 07:34:34.959	9.18	-51.32	715.7 ± 0.2	420.000	YES	NO	NO	121.76	NO
180119	2018-01-19 12:24:40.747	199.58	-50.41	402.7 ± 0.7	110.000	YES	NO	NO	98.08	NO
180128.0	2018-01-28 00:59:38.617	330.05	52.72	441.4 ± 0.2	51.000	YES	NO	NO	121.32	NO
180128.2	2018-01-28 04:53:26.796	329.86	-48.32	495.9 ± 0.7	66.000	YES	YES	NO	39.87	NO
180130	2018-01-30 04:55:29.993	4.21	-51.07	343.5 ± 0.4	95.000	-	-	-	-	NO
180131	2018-01-31 05:45:04.320	0.93	-50.47	657.7 ± 0.5	100.000	YES	NO	NO	116.37	NO
180212	2018-02-12 23:45:04.399	341.52	52.45	167.5 ± 0.5	96.000	IDLE	NO	NO	54.69	NO
180309	2018-03-09 02:49:32.990	10.90	-45.40	263.42 ± 0.01	13.120	YES	YES	NO	54.96	NO
180311	2018-03-11 04:11:54.800	337.30	-43.70	1570.9 ± 0.5	2.100	IDLE	-	-	45.81	NO
180315	2018-03-15 05:05:30.985	13.20	-20.90	479.0 ± 0.4	56.000	NO	NO	NO	148.08	NO
180324	2018-03-24 09:31:46.706	245.20	-20.50	431.0 ± 0.4	71.000	YES	NO	NO	126.04	NO
180417	2018-04-17 13:18:31.000	276.00	75.60	474.8	55.000	YES	NO	NO	105.53	NO
180430	2018-04-30 09:59:58.700	221.76	-4.61	264.1 ± 0.5	177.000	YES	NO	NO	168.04	NO
180515	2018-05-15 21:57:26.485	349.50	-64.90	355.2 ± 0.5	46.000	YES	YES	NO	60.12	NO
180525	2018-05-25 15:19:06.515	349.00	50.70	388.1 ± 0.3	300.000	NO	NO	NO	60.90	NO
180528	2018-05-28 04:24:00.900	258.80	-22.35	899.3 ± 0.6	32.000	YES	NO	NO	111.25	NO
180714	2018-07-14 10:00:08.700	14.80	8.72	1467.92 ± 0.3	1.850	NO	NO	NO	72.72	NO
180725.J0613+67	2018-07-25 17:59:32.813	147.00	21.00	715.98 ± 0.2	12.000	YES	NO	NO	114.43	NO
180727.J1311+26	2018-07-27 00:52:04.474	25.00	85.00	642.07 ± 0.03	14.000	YES	NO	NO	152.33	NO
180729.J0558+56	2018-07-29 00:48:19.238	115.00	61.00	317.37 ± 0.01	34.000	YES	YES	NO	61.89	NO
180729.J1316+55	2018-07-29 17:28:18.258	156.00	15.00	109.610 ± 0.002	9.000	YES	NO	NO	100.32	NO

Table 1 *continued*

Table 1 (*continued*)

ID	DATE UTC	LII (deg)	BII (deg)	DM and Error (cm^{-3}pc)	Radio Fluence (Jy ms)	Within MCAL FOV	Within GRID FOV	Within Super-A FOV	Off-axis Angle (deg)	Repeater
180730.J0353+87	2018-07-30 03:37:25.937	125.00	25.00	849.047 ± 0.002	50.000	YES	NO	NO	155.51	NO
180801.J2130+72	2018-08-01 08:47:14.793	109.00	15.00	656.20 ± 0.03	28.000	NO	NO	NO	42.06	NO
180806.J1515+75	2018-08-06 14:13:03.107	112.00	38.00	739.98 ± 0.03	24.000	YES	YES	NO	62.78	NO
180810.J0646+34	2018-08-10 17:28:54.614	180.00	14.00	414.95 ± 0.02	11.000	NO	NO	NO	64.62	NO
180810.J1159+83	2018-08-10 22:40:42.493	125.00	34.00	169.134 ± 0.002	17.000	YES	NO	NO	117.77	NO
180812.J0112+80	2018-08-12 11:45:32.872	123.00	18.00	802.57 ± 0.04	18.000	YES	NO	NO	153.02	NO
180814.J1554+74	2018-08-14 14:20:14.440	108.00	37.00	238.32 ± 0.01	25.000	YES	NO	NO	165.94	NO
180814.J0422+73	2018-08-14 14:49:48.022	136.00	16.00	189.38 ± 0.09	21.000	YES	NO	NO	116.42	YES
180817.J1533+42	2018-08-17 01:49:20.202	68.00	54.00	1006.840 ± 0.002	26.000	NO	NO	NO	20.36	NO
180908.J1232+74	2018-09-18 21:13:01.00	124.7	42.9	195.7 ± 0.9	2.700	YES	NO	NO	81.89	YES
180916.J0158+65	2018-09-16 10:15:19.802	129.70	3.70	349.2 ± 0.4	2.30	NO	NO	NO	155.08	YES
180924	2018-09-24 16:23:12.626	0.74	-49.41	361.42 ± 0.06	16.000	YES	NO	NO	139.88	NO
181016	2018-10-16 04:16:56.3	345.51	22.67	1982.8 ± 2.8	87.000	YES	NO	NO	86.53	NO
181017	2018-10-17 10:24:37.4	50.50	-47.00	239.97 ± 0.03	31.000	YES	NO	NO	73.46	NO
181017.J1705+68	2018-10-17 23:26:11.860	99.20	34.80	1281.9 ± 0.4	1.000	NO	NO	NO	3.95	YES
181030.J1054+73	2018-10-30 04:13:13.025	133.40	40.90	103.5 ± 0.7	7.300	YES	NO	NO	91.44	YES
181112	2018-11-12 17:31:15.483	342.60	-47.70	589.27 ± 0.03	26.000	YES	YES	NO	42.93	NO
181119.J12+65	2018-11-19 16:49:03.191	124.50	52.00	364.2 ± 1.0	1.800	NO	NO	NO	53.99	YES
181128.J0456+63	2018-11-28 08:27:41.740	146.60	12.40	450.2 ± 0.3	4.400	-	-	-	-	YES
181228	2018-12-28 13:48:50.1	253.39	-26.06	354.2 ± 0.9	24.000	YES	NO	NO	159.68	NO
190116.J1249+27	2019-01-16 13:07:33.833	210.50	89.50	444.0 ± 0.6	0.800	NO	NO	NO	48.06	YES
190222.J2052+69	2019-02-22 18:46:01.367	104.90	15.90	460.6 ± 0.1	-	YES	YES	NO	40.38	YES
190523	2019-05-23 06:05:55.815	117.03	44.00	760.8 ± 0.6	-	YES	NO	NO	111.84	NO
190102	2019-01-02 05:38:43.49184	312.654	-33.493	363.6 ± 0.3	14.000	YES	NO	NO	93.41	NO
190608	2019-06-08 22:48:12.88391	53.209	-48.530	338.7 ± 0.5	26.000	NO	NO	NO	169.31	NO
190611	2019-06-11 05:45:43.29937	312.935	-33.282	321.4 ± 0.2	10.000	YES	YES	NO	42.93	NO
190711	2019-07-11 01:53:41.09338	310.908	-33.902	593.1 ± 0.4	34.000	YES	NO	NO	142.35	NO

Note: No radio fluence available in FRBCAT for 190222.J2052+69 and 190523, and no DM error for 141113 and 180417.

phases in the period 2020 February–September. No X-ray emission has been detected simultaneously with radio burst activity and interesting constraints have been determined (Pilia et al. 2020; Tavani et al. 2020; Scholz et al. 2020). Recently, some high-energy counterpart searches for FRBs have been published (see Cunningham et al. 2019; Martone et al. 2019; Guidorzi et al. 2020; Marcote et al. 2020; Nicastro et al. 2021), based on the updated sample of sources in the FRBCAT catalog and reporting searches in timescales from 0.1 to 100 s in the X-ray/soft γ -ray bands. No significant detection was found, while average isotropic luminosity upper limits (ULs) have been set from Insight/HXMT data (40 keV–3 MeV), to $\sim 10^{49} - 10^{51} \text{ erg s}^{-1}$ for the most part of FRBs and $\sim 10^{47} \text{ erg s}^{-1}$ for Source 1 at 1 s integration, and 2 orders of magnitude higher at 0.1 s, while from Fermi and Swift/BAT data (8 keV–100 GeV) lower limits to the radio-to-X-ray flux ratio at $\sim 10^5 - 10^7 \text{ Jy ms cm}^2 \text{ erg}^{-1}$ have been set for the nonrepeating sources. In this paper, we report on a systematic search in AGILE archival data for MeV and GeV emission in coincidence with FRB radio detections. We searched for simultaneous or temporally close high-energy emission for a sample of 89 FRB sources selected from FRBCAT and from the CHIME/FRB telescope public online database, with the inclusion of recent FRB detections (Macquart et al. 2020). Most of these FRBs are nonrepeating.

In this paper, Section 2 presents a discussion of the different components making the observed DM of FRBs. Section 3 briefly presents the characteristics of the AGILE instrument. In Section 4 we present the FRB list and the details of our search analysis procedure. We discuss our measurements and their implications with respect to the radio fluences and DM distributions. In Section 4.1 and in Section 4.2 we report our main conclusions.

2. THE FRB DISPERSION MEASURE DECOMPOSITION AND THE CASE OF SOURCE 1

The DM of each FRB is given by the sum of the following components:

$$\text{DM} = \text{DM}_{\text{disk}} + \text{DM}_{\text{halo}} + \text{DM}_{\text{host}} + \text{DM}_{\text{IGM}} \quad (1)$$

where DM_{disk} and DM_{halo} are the Galactic disk and halo components, DM_{host} is the FRB source host galaxy component from disk and halo and all specific local gas, and DM_{IGM} is the intergalactic component. When no information on the local host component is known, we define the excess DM as $\text{DM}_{\text{ex}} = \text{DM}_{\text{host}} + \text{DM}_{\text{IGM}}$. The DM_{IGM} has a strong distance dependence, and DM_{host} could have a correlation with age (Macquart et al. 2020). The recently discovered CHIME/FRB and ASKAP FRBs include some sources having small total DM values only slightly in excess of the galactic contribution considering the available Galactic DM models (Cordes & Lazio 2002; Prochaska & Zheng 2019). Moreover, the recent precise localizations of a few FRBs (Chatterjee et al. 2017; Nicastro et al. 2021) allows to have a set of FRBs (nine sources) to compare the DM_{IGM} with the expected DM according to the intergalactic medium (IGM)-DM relation, $\text{DM} = 900 z \text{ pc cm}^{-3}$ (McQuinn 2014). Source 1 has a low value of DM_{ex} and has been recently localized with good precision by VLBI. It has been associated with a possible star-forming region in a massive spiral galaxy at redshift $z = 0.0337 \pm 0.0002$, corresponding to $149.0 \pm 0.9 \text{ Mpc}$ (M20). Knowing the distance, it is possible to estimate the DM_{host} for this source. After subtracting the DM_{disk} value and assuming a value of 50 pc cm^{-3} for DM_{halo} , we obtain $\text{DM}_{\text{ex}} \sim 100 \text{ pc cm}^{-3}$, but from $z = 0.0337$ we obtain $\text{DM}_{\text{IGM}} \sim 32 \text{ pc cm}^{-3}$ and consequently $\text{DM}_{\text{host}} \sim 68 \text{ pc cm}^{-3}$ (see Tavani et al. 2021). This source has the lowest DM_{IGM} among those with a certain localization.

the first repetition only; a complete analysis of all the repetitions is not included in this work. The AGILE satellite pointing direction rotates around the axis pointed towards the Sun; so the GRID and Super-A can obtain exposures of each FRB error circle at each satellite revolution not affected by Earth occultation or SAA passages (MCAL is only affected by Earth occultations; in the following we will indicate the unocculted region of the sky with "MCAL FOV"). We applied a procedure divided in two main steps: a first check of the eventual prompt emission, supposed to include a few seconds around T_0 taking into account the time delay due to dispersion of the radio frequency with respect to X-rays, and then a search for delayed or preceding emission on longer time scales. The initial check of the prompt coverage with the three detectors of a few seconds around T_0 to account for time delay due to dispersion value and its uncertainty (in the range $10^{-3} - 10 \text{ pc cm}^{-3}$) of each unocculted source has been executed, and we report the event coverage in dedicated columns of Table 1, indicating whether each source was within each detector's FOV at burst times (marked by the "Y" symbol, for "yes"). We determine that 15 FRBs were exposed at the radio event times within the GRID FOVs; instead only one (170107) was inside the Super-A FOV, while 54 events were inside the unocculted part of the sky for MCAL. In Figure 2 and 3, we show Aitoff plots in Galactic coordinates of the AGILE exposures of seven FRB events that occurred within the GRID FOV, in particular the one falling also within the Super-A one. In our analysis, we selected time intervals preceding and following the FRB radio times of arrival T_0 . We extended our searches to time intervals sufficiently large to take into account the radio dispersion delays that can amount to many seconds. In the following, we will describe analyses of two integrations timescales: (a) short timescales, below 1 hr; (b) long timescales, from

1 hr to 100 days. We will report the results with these timescales for the two AGILE detectors, MCAL and GRID.

4.1. Search for Hard X-ray/Soft γ -ray Emission

The AGILE/MCAL is a triggered detector, with an onboard trigger logic acting on different energy ranges and timescales (from $\sim 300 \mu\text{s}$ to $\sim 8 \text{ s}$). The submillisecond logic timescale allows MCAL to trigger on very short duration impulsive events. Moreover, the logic is capable of efficiently detecting long and short transients such as GRBs (Marisaldi et al. 2008; Galli et al. 2013) as well as terrestrial γ -ray flashes on millisecond and submillisecond timescales (Tavani et al. 2011; Marisaldi et al. 2015). A detailed discussion about MCAL triggering capabilities and UL evaluation is given in Casentini et al. (2020) and Ursi et al. (2019).

As soon as each FRB position becomes not occulted and accessible by MCAL, we carried out a search for transient X-ray emission on the six fixed integration timescales of the trigger logic in the 400 keV–100 MeV energy range at the data interval nearest in time, within $\pm 100 \text{ s}$. No significant triggered or untriggered detection was obtained by MCAL. We determined 3σ fluence UL values, reported in Table 2, with values ranging from $1.1 \times 10^{-8} \text{ erg cm}^{-2}$, on the submillisecond timescale, to $4.5 \times 10^{-7} \text{ erg cm}^{-2}$ on 8 s timescale, using a mean power law with photon index 1.5 as the spectral model.

4.2. Search for γ -ray Emission

We searched for γ -ray emission in the GRID detector data, applying two different types of analyses: the "GRB detection mode" (Giuliani et al. 2010; Verrecchia et al. 2017; Casentini et al. 2020) for short-timescale integrations of 10, 100 and 1000 s before and after the event T_0 , which allowed us to obtain flux ULs in the 50 MeV–10 GeV energy band; and the AGILE multi-source maximum likelihood (ML) analy-

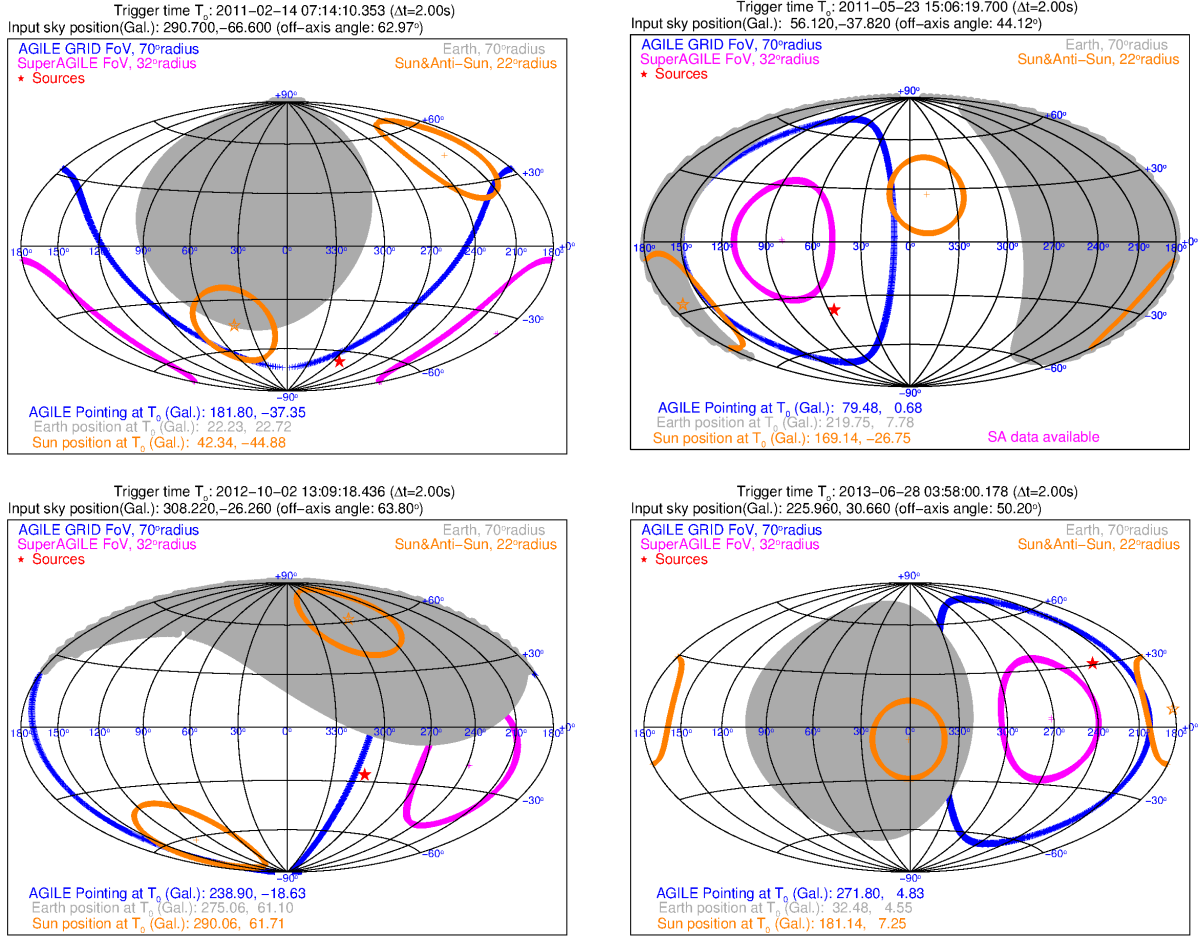


Figure 2. Top panels: the AGILE/GRID FoV map (in Galactic coordinates) at 110214 and 110523 T_0 (from left to right). Bottom panels: the FoV map at 121002 and 130628 T_0 . Source position is marked with a red star. Earth occulted region is in gray, while the Sun/anti-Sun inaccessible (to GRID and Super-A) regions are delimited with orange circles. The GRID FoV is shown with a blue circle, while the central part of the Super-A FoV is indicated with a magenta circle.

Table 2. Typical Fluence AGILE/MCAL 3σ Upper Limits (in erg cm^{-2})

Sub-ms	1 ms	16 ms	64 ms	256 ms	1024 ms	8192 ms
1.13×10^{-8}	1.29×10^{-8}	3.72×10^{-8}	4.97×10^{-8}	7.95×10^{-8}	1.59×10^{-7}	4.49×10^{-7}

sis (Bulgarelli et al. 2012) for long timescales, up to 100 days in the 100 MeV – 10 GeV band. The ULs were obtained for a mean power-law spectral model with photon index 2.0.

In the case of 110523, with a 100 s integration, applying the method described in Li & Ma (1983), we obtained a weak γ -ray signal spatially coincident with the FRB source at 3.2σ pretrial significance.

The typical AGILE/GRID γ -ray 2σ flux ULs for short and long integrations are shown in Figure 4 and Table 3, for the case of the first burst of the Source 2 repeater.

5. DISCUSSION

We notice that typical FRB excess DMs are in the range of 100–1000 pc cm^{-3} , primarily due to inter-galactic propagation of the radio

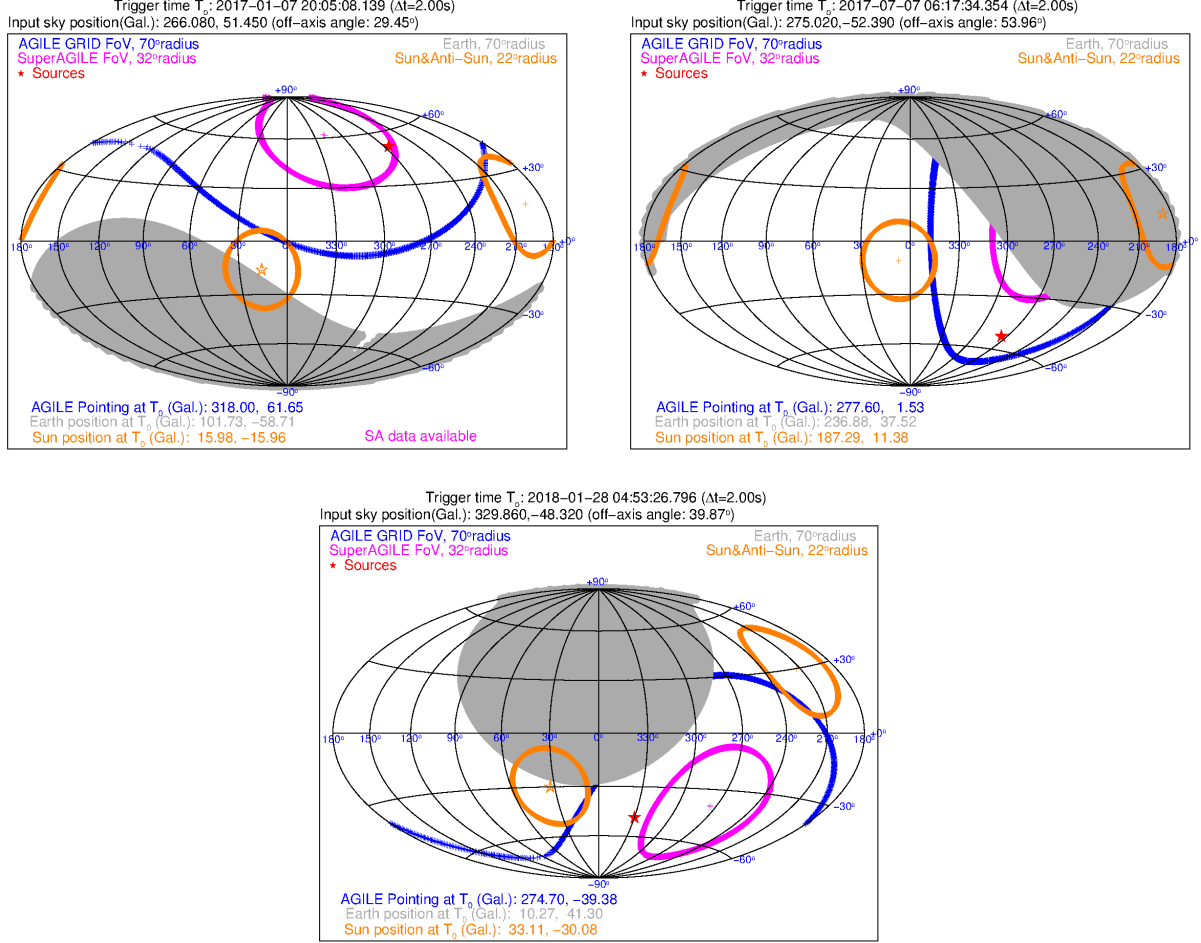


Figure 3. The AGILE/GRID FOV map (in Galactic coordinates) at 170107, 170707 (from left to right) and 180128.2 T_0 (bottom). Source position is marked with a red star.

Table 3. Typical Fluence AGILE/GRID 2σ Upper Limits (in $\text{erg cm}^{-2} \text{s}^{-1}$)

10 s	100 s	1000 s	1 day	10 days	100 days
1.80×10^{-7}	3.33×10^{-8}	6.67×10^{-9}	4.87×10^{-10}	3.53×10^{-11}	1.20×10^{-11}

signal (DM_{IGM} ; CC19), thus setting an extra-galactic scale for the FRB distances. Typical host-galaxy contributions to the DM (DM_{host} ; as for the case of our Galaxy) amount to values $\leq 100 \text{ pc cm}^{-3}$. Therefore, typical FRB source extrapolated distances are of the order of Gpc, except for a currently small number of FRBs with small DM excesses ($DM_{\text{IGM}} \leq 32 \text{ pc cm}^{-3}$) as shown in Table 4. This table includes also two sources having $DM_{\text{IGM}} < 100 \text{ pc cm}^{-3}$. Focusing on nearby FRB sources of Table 4,

we will consider the Source 1 distance as a distance UL for a typical scale of $d_{150\text{Mpc}} = d/(150 \text{ Mpc})$.

The observed emitted radio flux densities ($S_{\nu, Jy}$) of FRB events reported in Table 1 have typical values in the range 1–100 Jy, on millisecond timescales. These fluxes can be converted to energies considering the relation $E = S_{\nu} \times DM_{\text{IGM}}^2 \times K \times \Delta t_{-3} \times \Delta \nu_{\text{GHz}}$, where $F = S_{\nu, Jy}$ is the radio flux density in Jy, Δt_{-3} is the intrinsic temporal burst duration in units

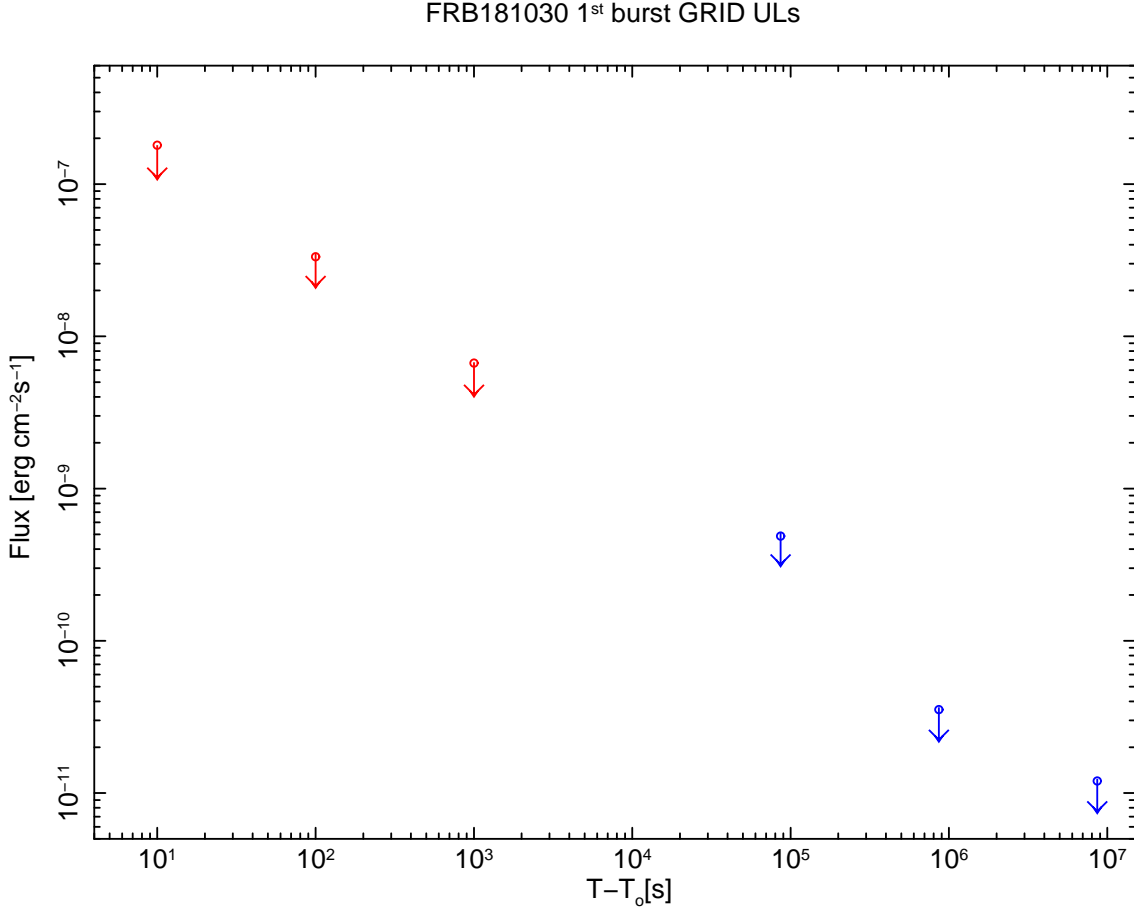


Figure 4. The typical AGILE/GRID γ -ray 2σ flux ULs obtained at the Source 2 position as a function of integration time. Integrations of 10, 100, and 1000 s are in the 50 MeV – 10 GeV energy band (in red), while those ranging from 1 to 100 days are in the 100 MeV – 10 GeV band (in blue).

of 1 ms, $\Delta\nu_{\text{GHz}}$ is the bandwidth in units of GHz and K is a constant for the conversion from DM_{IGM} to distance in parsecs. In Figure 5 we show the values of the quantities $F \times \text{DM}_{\text{ex}}^2$ (which is based on measured values of DM with the Galactic plane contribution subtracted) and of $F \times \text{DM}_{\text{IGM}}^2$ (which is a deduced quantity; see Table 4). The values of DM_{IGM}^2 are evaluated with the assumption reported in Section 2 and $\text{DM}_{\text{host}} = 50 \text{ pc cm}^{-3}$ for sources for which the distance is not known; consequently, some of the sources in Table 4 have negative values of this quantity. In Figure 6, we show the

observed FRB radio spectral fluences and the deduced isotropic FRB radio energies. The latter quantities turn out to be in the range $\sim 10^{37} - 10^{43} \text{ erg}$.

Our fluence UL F' in the millisecond range at near-MeV energies has the typical value of $F'_{\text{MeV,UL}} = 10^{-8} \text{ erg cm}^{-2}$ (or $10^{-7} \text{ erg cm}^{-2}$ in the range of seconds) for all the FRBs exposed by AGILE/MCAL, in particular for those of Table 4 (except 171020, which was occulted). This fluence UL translates into an UL for the isotropically MeV-radiated energy $E_{\text{MeV,UL}} \simeq (2.7 \times 10^{46} \text{ erg}) \text{ d}_{150\text{Mpc}}^2$ (or $\simeq (4.0 \times 10^{47} \text{ erg}) \text{ d}_{150\text{Mpc}}^2$

Table 4. Estimated parameters of FRBs with low DM_{IGM} (assuming $DM_{\text{halo}} = 50 \text{ pc cm}^{-3}$).

ID	Tel. ¹	DM ²	DM _{gal}	DM _{host}	DM _{IGM} ³	z_{est} ⁴	d_{est} ⁵	W. ⁶	AGILE Cov. ⁷
			(pc cm ⁻³)				(Mpc)	(ms)	
171020	A	114.1 ± 0.2	38.0	< 32	< 32	< 0.0340	< 150	3.20	NNN
171213	A	158.6 ± 0.2	36.0	< 41	< 32	< 0.0340	< 150	1.50	YNN
180430	A	264.1 ± 0.5	165.4	50	< 32	< 0.0340	< 150	1.20	YNN
180729.J1316+55	C	109.61 ± 0.002	31.0	< 32	< 32	< 0.0340	< 150	0.12	YNN
180810.J1159+83	C	169.134 ± 0.002	47.0	50	< 32	0.0246	< 150	0.28	YNN
180814.J0422+73(R)	C	189.38 ± 0.09	87.0	< 20	< 32	< 0.0340	< 150
181030.J1054+73(R)	C	103.5 ± 0.7	40.0	< 32	< 32	< 0.0340	< 150
180916.J0158+65(R)	C	348.8 ± 0.2	200.0	68	32.0 ⁺	0.0337 ⁺	149 ⁺
110214	P	168.9 ± 0.5	31.1	50	37.8	0.0420	177	1.90	YYN
170707	A	235.2 ± 0.6	36.0	50	99.2	0.1102	465	3.50	YYN

(R) Repeater FRBs.

(1) Radio telescopes, "C" for CHIME/FRB, "A" for ASKAP and "P" for Parkes.

(2) Observed dispersion measure values (Petroff et al. 2016).

(3) The contribution to DM from the IGM obtained by subtracting the Galactic plane contribution (depending on the sky position) and the Galactic halo (which we assumed to be equal to 50 pc cm^{-3} ; Prochaska & Zheng 2019) plus host galaxy contribution (the latter value has been assumed to be equal to 50 pc cm^{-3} except for source 1 whose distance is known). However sources with low DM have uncertain DM_{host} value (using the previous assumptions would bring to negative values) so we assume they should have a DM_{host} value lower than that of Source 1.

(4,5) Estimated redshift according to the IGM-DM relation in McQuinn 2014 and the corresponding distance.

(6) Radio burst scattering-corrected width.

(7) AGILE event spatial coverage within the three detectors' FOV, according to Table 1 (MCAL, GRID and SA, respectively), where "Y" for "Yes" and "N" for "No", while we do not report the coverage for R-FRB, indicated with ellipses.

(+) The value of DM_{IGM} of the repeater Source 1 is known (Marcote et al. 2020; Tavani et al. 2020).

for the second timescale). Obviously, the total emitted energy can be smaller than the isotropic equivalent when taking into account the eventual beaming effect.

This UL is relevant because it is of the same order of magnitude of the 200 ms long first peak of the 2004 "giant flare" from SGR 1806-20 (with an emitted energy $\sim 3 \times 10^{46}$ erg; Palmer et al. 2005; Hurley et al. 2005). The lack of MeV detections for the FRBs of Table 4 translates into the absence of X-ray bursts larger than the most intense giant flare from a Galactic magnetar. Our result is very significant in light of the recent discovery of a giant radio burst from the Galactic magnetar SGR 1935+2154 (Mereghetti 2020; Bochenek et al. 2020a,b; Scholz 2020; Scholz et al. 2020; Li et al. 2020). FRB-like

radio pulses are therefore associable to magnetars (e.g., Tavani et al. 2020; Katz 2020), and we might expect powerful X-ray emission in coincidence with FRBs. This expectation is based on the energetics of the radio emission from FRBs as deduced from Fig. 5 that requires a source of energy presumably larger than that available in observed Galactic magnetars, when considering those sources having high measured DM values, so are probably distant. This source might be a fraction of the magnetic field energy that for a neutron star of radius $R = 10^6$ cm is $E_B \sim R^3 B_*^2 / 6 \sim 2 \times 10^{49} B_{*,16}^2$ erg, where $B_{*,16}$ is the internal magnetic field in units of 10^{16} G, where radio emission can be triggered by neutron star magnetic field instabilities or magnetospheric particle acceleration phenomena (as dis-

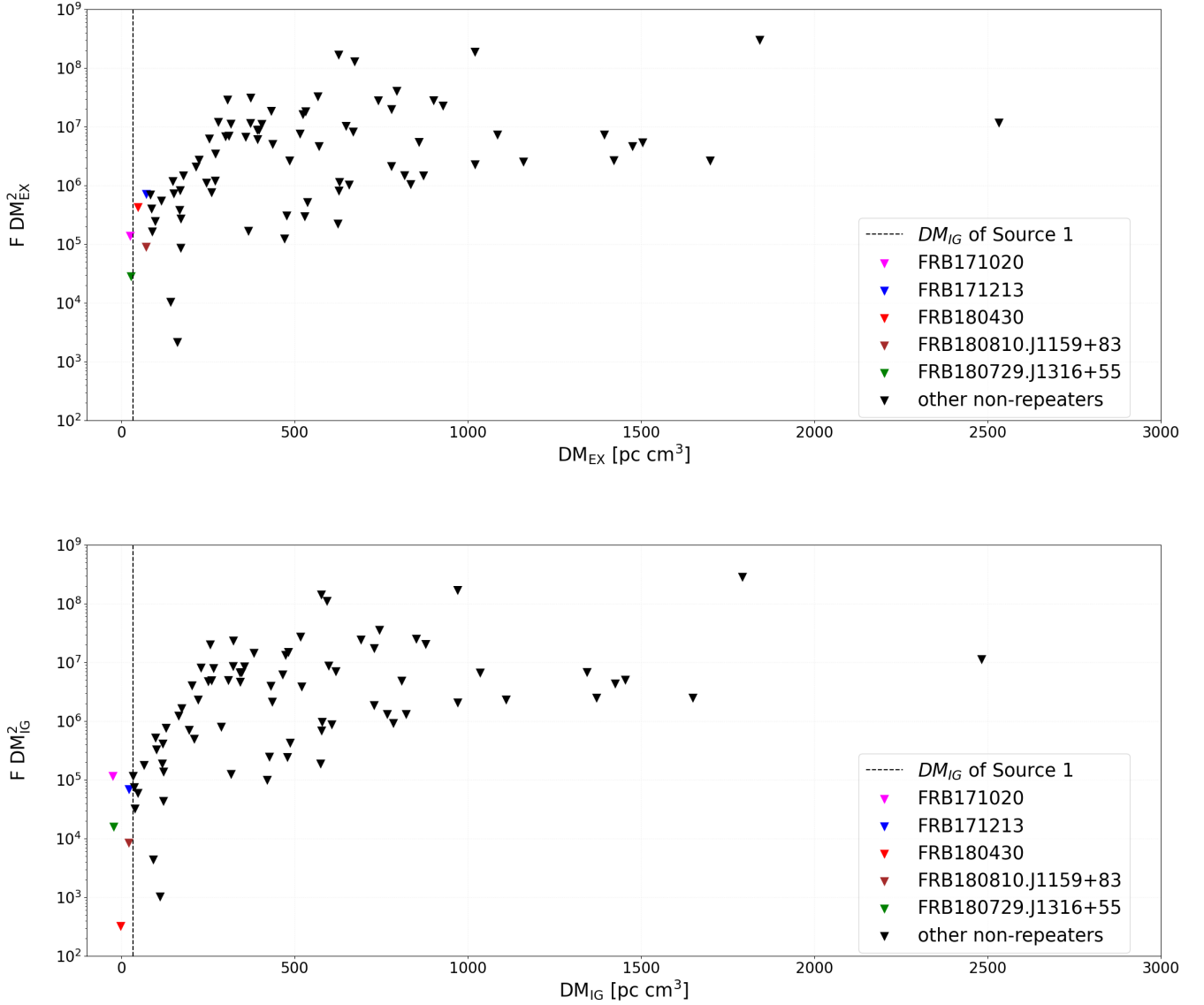


Figure 5. The radio flux times excess DM (DM_{ex} ; top panel) squared as a function of DM_{ex} , and radio flux times the DM_{IGM} (bottom panel) squared as a function of DM_{IGM} for the nonrepeater bursts sample, where DM_{ex} and DM_{IGM} are calculated subtracting from the observed DM the Galactic disk and halo components only and the DM_{host} too, respectively.

cussed in Thompson & Duncan 1996). It is interesting to note that in the case of SGR 1806-20 (with a magnetic field deduced from the magnetar spindown $B_{*,16} \simeq 0.2$; Kaspi 2017) the giant outburst flare energy of 3×10^{46} erg corresponds to a fraction of 2.5% of the total energy E_B . We therefore can expect detectable X-ray and MeV flaring activity near the UL value $E_{\text{MeV,UL}}$, or above, from FRBs if magnetars constitute the

physical sources associated with the majority of FRBs of Table 4.

A variety of FRB models discuss the possibility of X-ray and γ -ray emission from magnetar sources associated with coherent radio pulses (see CC19, Petroff et al. 2019 and Platts et al. 2019 for a 2019 summary). The synchrotron maser modeling of FRB radio flares has been recently applied to the newly discov-

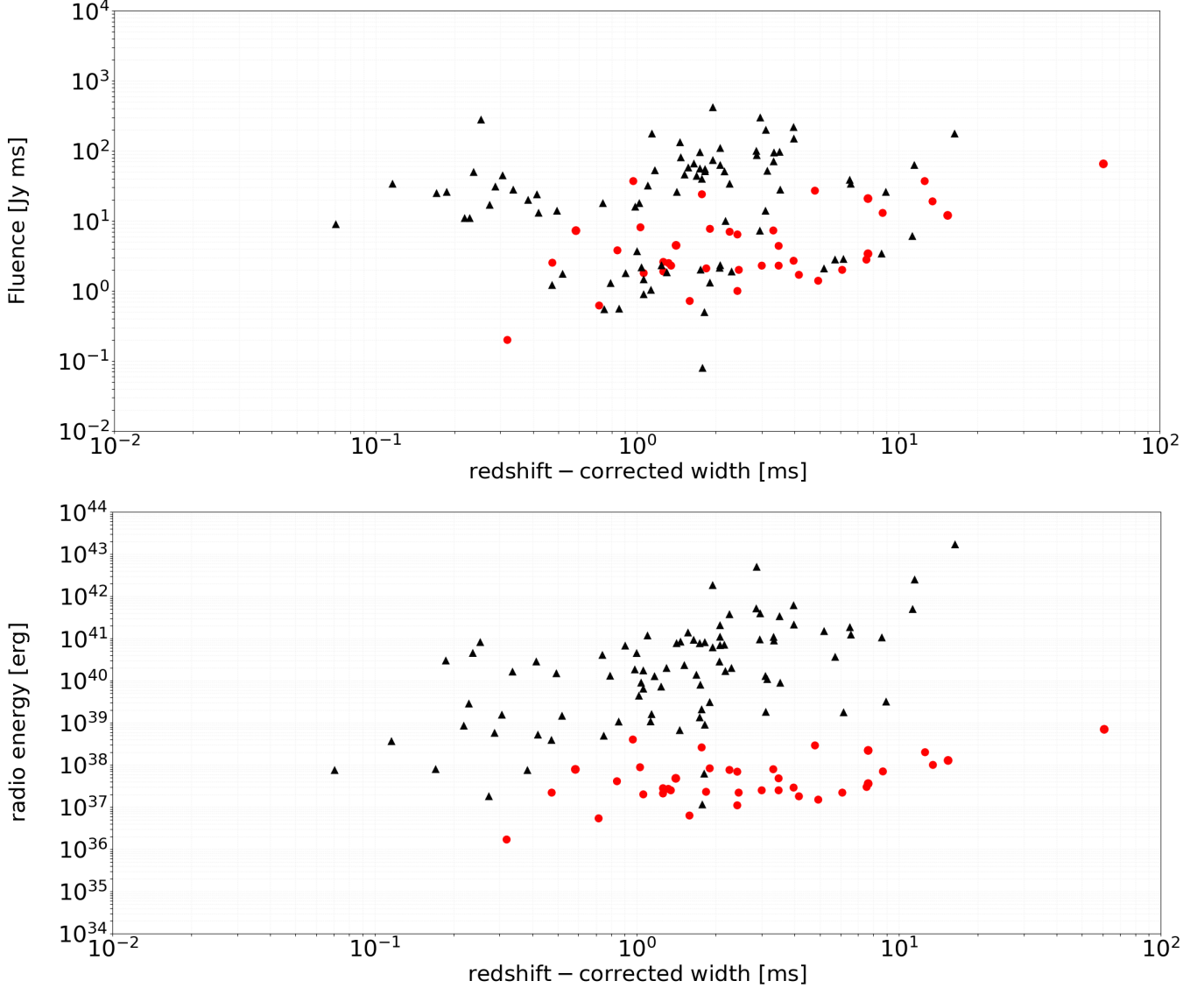


Figure 6. The radio fluence (top panel) and isotropically emitted energy (bottom panel) vs. the redshift-corrected time widths for the same sample of nonrepeating FRBs (black triangles) and for a sample of R-FRBs (red circles). FRB radio data (typically in the 400 MHz—1.5 GHz band) and DM information are from FRBCAT (Petroff et al. 2016). Distances of non localized FRBs have been derived from their intergalactic DM (DM_{IGM}) once the Galactic disk and halo contributions have been subtracted from the observed DM, together with the host galaxy one (this latter value has been assumed to be such that $DM_{\text{halo}} + DM_{\text{host}} = 50 + 50 = 100 \text{ pc cm}^{-3}$, in good agreement with the direct measurement of Source 1).

ered CHIME/FRB burst repeaters (Margalit et al. 2020b) and to the comparison of FRBs with the SGR 1935+2154 1 millisecond radio flare detected on April 28th (Scholz 2020; Bochenek et al. 2020a; Scholz et al. 2020; Mereghetti 2020; Bochenek et al. 2020b; Li et al. 2020) and with other magnetar X-ray bursts (Mar-

galit et al. 2020a). The simultaneous radio and X-ray burst detections of SGR 1935+2154 allow us to obtain the radio-to-X-ray fluence ratio $E_{\text{radio}} / E_X \sim 10^{-5}$, where $E_{\text{radio}} \sim 2 \times 10^{35} \text{ erg}$ and $E_X \sim 8 \times 10^{39} \text{ erg}$ (with the assumption of a distance of 10 kpc, Tavani et al. 2021). It is a single event but indicative of a physical

phenomenon that has to produce simultaneous X-ray emission, together with unabsorbed radio pulses. The decelerating maser blast wave model (Beloborodov 2017; Metzger et al. 2019), based on the observed parameters of the radio burst alone, leads us to infer the intrinsic energy of the SGR 1935+2154 flare to be $E_{\text{flare}} \sim 10^{40} \text{ erg } (\xi / 10^{-3})^{-4/5} (W/5\text{ms})^{-1/5} d_{10}^2$, where ξ is the intrinsic synchrotron maser efficiency, supposed to be $\sim 10^{-2} - 10^{-3}$ (for moderate magnetization), $d_{10} = d/10 \text{ kpc}$, and W is the 1.4 GHz burst duration. This energy is $E_{\text{flare}} \simeq E_X$ and the expected $E_{\text{radio}} / E_{\text{flare}}$ is of the same order as the observed one, 10^{-5} . Moreover, delayed X-ray radiation is expected: the “afterglow” peak frequency is set by synchrotron emission, and in the model of a decelerating ultrarelativistic blastwave, it corresponds to $E_{\text{peak}} \sim h\nu_{\text{sync}} \simeq 160 \text{ keV } \sigma_{-1}^{1/2} (W/5\text{ms})^{1/10} (t/5\text{ms})^{-3/2} d_{10}^2$ and so $E_{\text{peak}} = 10 - 100 \text{ keV}$, with t the time from the flare peak and $\sigma = 10^{-1} \sigma_{-1}$ the medium magnetization parameter (Metzger et al. 2019). We consider a fast cooling synchrotron spectrum with an exponential cutoff at ν_{sync} , so that $F_{\text{peak}} \propto E_{\text{flare}}$, where F_{peak} is the fluence at E_{peak} . This range of emitted radiation is compatible with the observations of SGR 1935+2154. However, this model predicts a level of prompt X-ray emission significantly lower than the giant flare of SGR 1806-20, and consequently, it does not predict detectable high-energy emission from the FRBs of Table 4.

Prompt and delayed γ -ray emission can be considered as well. A deceleration blast wave model leads to $E_{\text{peak}} \geq \text{MeV} - \text{GeV}$ for millisecond timescale emissions in the γ -ray band (Margalit et al. 2020a); these expected short bursts are different from the giant Galactic magnetar soft γ -ray flares lasting several hundreds of milliseconds. The synchrotron maser model thus predicts that radio flares might

be followed by emissions also in the γ -ray band; the fluences (in MeV–GeV band) calculated for SGR 1935+2154 should be of the order of $10^{-12} \text{ erg cm}^{-2}$ (Margalit et al. 2020b). The FRB phenomenon might lead to high-energy emission on long timescales, from days to months/years. In this hypothesis AGILE/GRID observations of the FRBs of Table 1 (marked by “YES” in the GRID column) allowed us to set γ -ray ULs at different integration timescales ranging from tens of seconds up to hundreds of days. The longest timescale flux ULs for 100-day integrations are of the order of $\sim (1 - 2) \times 10^{-11} \text{ erg cm}^{-2} \text{ s}^{-1}$ above 100 MeV. For FRBs with small excess DM, this UL corresponds to the isotropic luminosity limit

$$L_{\gamma, UL} \simeq (2 - 5) \times 10^{43} d_{150 \text{ Mpc}}^2 \text{ erg s}^{-1}. \quad (2)$$

Eq. 2 indicates that delayed γ -ray emission from FRBs is unlikely to be detected also for distances smaller by one order of magnitude compared to Source 1.

6. CONCLUSIONS

In this paper we report the results of a systematic search for high-energy emission in AGILE data from FRBs. Outflows are expected to be leptonic; hadrons, if any, may lead to neutrino emission in case of near-magnetar or interstellar shocks, but we do not believe this is the case under the circumstances of situations leading to strong radio pulses. Our search for MeV and GeV emission associated with FRBs did not produce a positive detection among the 89 FRBs that were accessible to our investigation. Interestingly, for a subsample of these FRBs, 15 events, we could determine the lack of detectable emission in the MeV range at a level that is close to the giant flare emission from the magnetar SGR 1806-20. Our ULs are particularly relevant for FRB sources with low intergalactic DM, i.e., presumably located at relatively small distances (smaller than 150 Mpc),

whose parameters are shown in Table 4. Currently, the distance out to which we can exclude an MeV flare in the millisecond timescale range similar to SGR 1806-20 for FRBs is 100 Mpc. Furthermore, we obtain long-timescale γ -ray luminosity limits reaching the relevant value of $\sim 10^{43} d_{150 \text{ Mpc}}^2 \text{ erg s}^{-1}$.

Recently, other high-energy counterpart searches for FRBs have been reported, with results qualitatively similar to those reported here (see Cunningham et al. 2019; Martone et al. 2019; Marcote et al. 2020; Guidorzi et al. 2020), such as isotropic γ -ray luminosity limits $\geq 10^{46} \text{ erg s}^{-1}$ at 1 ms timescale. The search for X-ray, as well as MeV and GeV, emissions from FRBs should continue as more events are discovered and, hopefully, smaller distances are applicable.

The recent breakthrough discovery of a giant double-peaked radio burst from the Galactic magnetar SGR 1935+2154 (Scholz et al. 2020; Bochenek et al. 2020b) was announced when this work was in its final form. The detection of a structured X-ray burst associated with the giant radio burst from SGR

1935+2154 (Mereghetti 2020; Tavani et al. 2021; Ridnaia 2020; Li et al. 2020) confirms that high-energy emission can be associated with coherent submillisecond radio bursts from a magnetar. These data are of crucial relevance for resolving the question of the ultimate origin of a class of, if not all, FRBs. Future investigations on the possible link between FRB sources and highly magnetized neutron stars will be presented elsewhere.

Acknowledgments:

This investigation was carried out with partial support by the ASI grant no. I/028/12/05. We would like to acknowledge the financial support of ASI under contract to INAF: ASI 2014-049-R.0 to ASI-SSDC. We thank the anonymous referee for the useful comments that helped to improve the manuscript. F.V. dedicates this work to his late father Giorgio.

REFERENCES

- Barbiellini, G., Fedel, G., Liello, F., et al. 2002, NIM A, 490, 146
- Beloborodov, A. M. 2017, ApJL, 843, L26
- Bochenek, C., Kulkarni, S., Ravi, V., et al. 2020a, ATel, 13684, 1
- Bochenek, C., Kulkarni, S., Ravi, V., et al. 2020b, Natur, 587, 59
- Bulgarelli, A. 2019, ExA, 48, 199
- Bulgarelli, A., Chen, A.W., Tavani, M., et al. 2012, A&A, 540, A79
- Bulgarelli, A., Trifoglio, M., Gianotti, F., et al. 2014, ApJ, 781, 19
- Casentini, C., Verrecchia, F., Tavani, M., et al. 2020, ApJL, 890, L32
- Chatterjee, S., Law, C. J., Wharton, R. S., et al. 2017, Natur, 541, 58
- CHIME/FRB Collaboration, Amiri, M., Bandura, K., Bhardwaj, M., et al. 2019a, Natur, 566, 230
- CHIME/FRB Collaboration, Amiri, M., Bandura, K., Bhardwaj, M., et al. 2019b, Natur, 566, 235
- CHIME/FRB Collaboration, Andersen, B. C., Bandura, K., Bhardwaj, M., et al. 2019c, ApJL, 885, 24 (C19)
- CHIME/FRB Collaboration, Amiri, M., Andersen, B. C., Bandura, K., Bhardwaj, M., et al. 2020, Natur, 582, 351 (C20)
- Cordes, J. M., and Chatterjee, S. 2019, ARA&A, 119, 161101 (CC19), doi:10.1146/annurev-astro-091918-104501
- Cordes, J. M., & Lazio, T. J. W. 2002, arXiv preprint astro-ph/0207156
- Cunningham, V., Cenko, S. B., Burns, E., et al. 2019, ApJ, 879, 40
- Feroci, M., Costa, E., Soffitta, P., et al. 2007, NIM A, 581, 728

- Fonseca, E., Andersen, B.C., Bhardwaj, M., et al. 2020, *ApJL*, 891, L6
- Galli, M., Marisaldi, M., Fuschino, F., et al. 2013, *A&A*, 553, A33
- Giuliani, A., Fuschino, F., Vianello, G., et al. 2010, *ApJL*, 708, L84
- Guidorzi, C., Marongiu, M., Martone, R., et al. 2020, *A&A*, 637A, 69
- Hurley, K., Boggs, S. E., Smith, D. M., et al. 2005, *Natur*, 434, 1098
- Kaspi, V. M., Beloborodov, A. M. 2017, *ARA&A*, 55, 261
- Katz, J. I. 2019, *MNRAS*, 487, 491
- Katz, J. I. 2020, *MNRAS*, 499, 2319
- Labanti, C., Marisaldi, M., Fuschino, F., et al. 2009, *NIMPA*, 598, 470
- Li, C. K., Lin, L., Xion, S. L., et al. 2020, *Nature Astronomy*, 5, 378
- Li, T. & Ma, Y. 1983, *ApJ*, 272, 317
- Lorimer, D. R., Bailes, M., McLaughlin, M. A., Narkevic, D. J., & Crawford, F. 2007, *Science*, 318, 777
- Macquart, J. P., Prochaska, J. X., McQuinn, M., et al. 2020, *Natur*, 581, 391
- Marcote, B., Nimmo, K., Hessels, J. W. T., et al. 2020, *Natur*, 577, 190
- Margalit, B., Beniamini, P., Sridhar, N., et al. 2020a, *ApJL*, 899, L27
- Margalit, B., Metzger, B. D., Sironi, L., et al. 2020b, *MNRAS*, 494, 4627
- Marisaldi, M., Argan, A., Ursi, A., et al. 2015, *GeoRL*, 42, 9481
- Marisaldi, M., Labanti, C., Fuschino, F., et al. 2008, *A&A*, 490, 1151
- Martone, R., Guidorzi, C., Margutti, R., Nicastro, L., Amati, L., et al. 2019, *A&A*, 631, A62
- McQuinn, M. 2014, *ApJ*, 780, L33
- Mereghetti, S., Savchenko, V., Ferrigno, C., et al. 2020, *ApJL*, 829, L29
- Metzger, B. D., Margalit, B., and Sironi, L. 2019, *MNRAS*, 485, 4091
- Nicastro, L., Guidorzi, C., Palazzi, E., et al. 2021, *Univ*, 7, 76
- Palmer, D.M., Barthelmy, S., Gehrels, N., et al. 2005, *Natur*, 434, 1107
- Perotti, F., Fiorini, M., Incorvaia, S., Mattaini, E., & Sant’Ambrogio, E. 2006, *NIMPA*, 556, 228
- Petroff, E., Barr, E. D., Jameson, A., et al. 2016, *PASA*, 33, e045
- Petroff, E., Hessels, J. W. T. & Lorimer, D. R. 2019, *A&ARv*, 27, 4.
- Pilia, M., Burgay, M., Possenti, A., et al. 2020, *ApJL*, 896, L40, [arXiv:2003.12748](https://arxiv.org/abs/2003.12748)
- Pittori, C. 2013, *NuPhS*, 239, 104
- Platts, E., Weltman, A., Walters, A., et al 2019, *PhR*, 821, 1, <http://frbtheorycat.org>.
- Pleunis, Z., Michilli, D., Bassa, C.G., et al 2021, *ApJL*, 911, L3
- Prochaska, J. X., & Zheng, Y., 2019, *MNRAS*, 485, 648
- Ridnaia, A., Svinkin, D., Frederiks, D., et al. 2020, *NatAs*, 5, 372
- Scholz, P., 2020, *ATel*, 13681, 1
- Scholz, P., Cook, A., Cruces, M., et al. 2020, *ApJL*, 901, 165
- Spitler, L. G., Scholz, P., Hessels, J. W. T., et al. 2016, *Natur*, 531, 202
- Tavani, M. 2019, *RLSFN*, 30, 13
- Tavani, M., Barbiellini, G., Argan, A., et al. 2009, *A&A*, 502, 995
- Tavani, M., Casentini, C., Ursi, A., et al. 2021, *NatAs*, 5, 401
- Tavani, M., Marisaldi, M., Labanti, C., et al. 2011, *Physical Review Letters*, 106, 018501
- Tavani, M., Verrecchia, F., Casentini, C., et al. 2020, *ApJL*, 893, L42
- Thompson, C. & Duncan, R. C. 1996, *ApJ*, 473, 322
- Ursi, A., Tavani, M., Verrecchia, F., et al. 2019, *ApJ*, 871, 27
- Verrecchia, F., Tavani, M., Bulgarelli, A., et al., 2019, *RLSFN*, 30, 71
- Verrecchia, F., Tavani, M., Donnarumma, I., et al. 2017, *ApJL*, 850, L27